
Learning production functions for supply chains with graph neural networks

Serina Chang¹, Zhiyin Lin¹, Benjamin Yan¹, Swapnil Bembde², Qi Xiu², Chi Heem Wong^{1,2},
Yu Qin^{2,3}, Frank Kloster², Alex Luo², Raj Palleti^{1,2}, and Jure Leskovec¹

¹Stanford University, Department of Computer Science

²Hitachi America, Ltd.

³Tulane University

Abstract

The global economy relies on the flow of goods over supply chain networks, with nodes as firms and edges as transactions between firms. While we may observe these external transactions, they are governed by unseen *production functions*, which determine how firms internally transform the input products they receive into output products that they sell. In this setting, it can be extremely valuable to infer these production functions, to better understand and improve supply chains, and to forecast future transactions more accurately. However, existing graph neural networks (GNNs) cannot capture these hidden relationships between nodes' inputs and outputs. Here, we introduce a new class of models for this setting, by combining temporal GNNs with a novel inventory module, which learns production functions via attention weights and a special loss function. We evaluate our models extensively on real supply chains data, along with data generated from our new open-source simulator, SupplySim. Our models successfully infer production functions, with a 6-50% improvement over baselines, and forecast future transactions on real and synthetic data, outperforming baselines by 11-62%.

1 Introduction

Supply chains form the backbone of the global economy and disruptions can have enormous consequences, costing trillions of dollars (Baumgartner et al., 2020) and risking national security (The White House, 2021). Thus, modeling supply chains and predicting how they will evolve, especially under shocks, are essential. To model supply chains, we can represent them as temporal (or dynamic) graphs, where nodes are firms and edges represent time-varying transactions between firms. A unique feature of these graphs is that they are governed by underlying *production functions*: firms receive input products (e.g., wheels) from other firms, internally transform those inputs into outputs (e.g., cars) via production functions, then sell those output products to other firms or consumers (Carvalho and Tahbaz-Salehi, 2019). These production functions dictate which firms are connected to each other, as well as the timing of transactions across the network. For example, if a firm experiences a shortage in an input, its production of outputs that rely on that input will be disrupted, but it can continue to produce other outputs for some time. Conversely, if a firm needs to produce more of a particular output, due to a change in demand, it will increase its orders of the inputs required to produce that output, but orders for other inputs may remain unchanged.

Despite growing interest in developing graph neural networks (GNNs) for temporal graphs (Huang et al., 2023; Longa et al., 2023), temporal graphs governed by production functions—which we term *temporal production graphs* (TPGs) in this work—have not yet been explored. Beyond supply chains, examples also appear in biological domains, such as enzymes producing metabolites within

metabolic pathways, or in organizations, where teams rely on inputs from other teams to produce their outputs (e.g., engineers interfacing with product designers). TPGs introduce new challenges compared to other temporal graphs, such as the need to infer the production functions. Inferring a TPG’s production functions can help us better understand the graph’s mechanisms and intervene more effectively, such as identifying bottlenecks in supply chains and proposing plausible solutions to improve efficiency and sustainability (Aigner and Chu, 1968; Coelli et al., 2005). Furthermore, even standard tasks, like link prediction, may be complicated under TPGs. For example, while standard temporal GNNs might capture disruptions generally propagating across connected firms in supply chains, they will miss the specific connections between each firm’s inputs and outputs and, under a shortage of inputs, not be able to precisely predict which outputs will be affected.

To fill this gap, here we introduce a *new class of GNNs* designed for TPGs, focusing on two objectives: (1) learning the graph’s internal production functions, (2) predicting its future edges. Prior temporal GNNs have focused primarily on the second objective, but are not designed for the first. Our models support both objectives, by combining temporal GNNs with a novel inventory module, which learns production functions by explicitly representing each firm’s time-varying inventory and updating it based on attention weights that map external supply to internal consumption. Our module can be combined with any GNN; to demonstrate this, here we combine it with two popular temporal GNNs, Temporal Graph Network (TGN) (Rossi et al., 2020) and GraphMixer (Cong et al., 2023), which we also extend in important ways. In this work, we have rare access to real-world transaction-level supply chains data, which we use to evaluate our models. We also build a new open-source simulator, SupplySim, which generates realistic supply chain data that matches the real data on key characteristics. Our simulator enables us to share data, encourage further research development on TPGs, and test models under controlled and varied settings (e.g., supply shocks, missing data). In summary, our contributions are:

1. **Problem:** a new graph ML problem setting, *temporal production graphs* (TPGs), where each node’s edges are related via unobserved production functions,
2. **Models:** a new class of models for TPGs, which combine temporal GNNs with a novel inventory module to jointly learn production functions and forecast future edges,
3. **Data:** an open-source simulator, SupplySim, which generates realistic supply chain data and enables model testing under a wide variety of settings,
4. **Results:** experiments on two real-world supply chain datasets and synthetic datasets from SupplySim, showing that our models effectively learn production functions (outperforming baselines by 6-50%) and forecast future edges (outperforming baselines by 11-62%).

While we focus on supply chains in this work, our models could be applied or easily extended to other TPGs. Our work pushes forward the frontier of graph ML and its application to real-world problems, by highlighting a new type of real-world graph and introducing new methods to handle them.¹

2 Learning from temporal production graphs

2.1 Problem definition

We define a new graph ML setting called *temporal production graphs* (TPGs), illustrated in Figure 1a. TPGs are directed graphs with time-varying edges and potentially a time-varying set of nodes. What differentiates TPGs from other temporal graphs is that, in a TPG, each node’s in-edges represent inputs to some internal production function, which are transformed into outputs, represented by the node’s out-edges. In this work, we focus on supply chain networks, as a canonical example of TPGs. We are given a set of transactions \mathcal{T} between firms where, for each transaction, we know its timestamp, supplier firm, buyer firm, product sold, and amount sold. We represent this data as a heterogeneous temporal graph, $G_{\text{txns}} = \{\mathcal{N}, \mathcal{E}\}$, where the nodes \mathcal{N} consist of n firm nodes and m product nodes and the edges are $\mathcal{E} := \{e(s, b, p, t)\}$, where $e(s, b, p, t)$ is a *hyperedge* between supplier firm s , buyer firm b , and product p , representing a transaction between them at time t .

In this setting, production functions define how firms internally transform the products that they buy into products that they supply. Specifically, the function $\mathcal{F}_p : \mathbb{R}_+ \rightarrow \mathbb{R}_+^m$ for product p defines how

¹Our code to run all experiments, simulator SupplySim, and synthetic datasets are available at <https://github.com/snap-stanford/supply-chains/tree/tgb>.

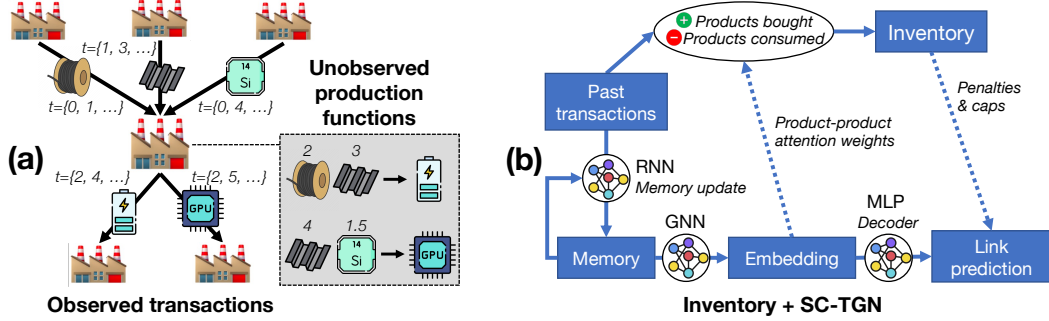


Figure 1: **(a)** Illustration of our problem setting: we observe time-varying transactions between firms and do not observe production functions within firms. Our goals are to learn the production functions and predict future transactions. **(b)** Example of our model architecture, combining our inventory module with our extended version of TGN, SC-TGN.

much of each product is necessary to make k amount of p (e.g., a car requires four wheels). The set of production functions define a *production graph*, G_{prod} , which is a directed acyclic graph where there is an edge from products p_1 to p_2 if p_1 is required to make p_2 .² Given the set of transactions \mathcal{T} , and the resulting temporal graph G_{txns} , our goals are two-fold: (1) to infer G_{prod} , which is entirely unobserved, (2) to predict future transactions, i.e., future hyperedges in G_{txns} .

2.2 Model architecture

To learn from TPGs, we introduce a new class of models that combine temporal GNNs with a novel inventory module to jointly learn production functions and predict future edges. First, we describe our inventory module, which can either operate as a stand-alone model or be attached to any GNN. Second, we describe extended versions of two popular temporal GNNs, Temporal Graph Network (Rossi et al., 2020) and GraphMixer (Cong et al., 2023), which we refer to as SC-TGN (shown in Figure 1b) and SC-GraphMixer, respectively, with SC standing for supply chain.

2.2.1 Inventory module

The basic idea of our inventory module is that it explicitly represents each firm’s inventory of products, and it adds and subtracts from the inventory based on products bought and products consumed, respectively. Let $\mathbf{x}_i^{(t)} \in \mathbb{R}_+^m$ represent firm i ’s inventory at time t . We compute the total amount of product p bought by firm i at time t as

$$\text{buy}(i, p, t) = \sum_{e(s,i,p,t) \in \mathcal{E}} \text{amt}(s, i, p, t), \quad (1)$$

where $\text{amt}(s, i, p, t)$ represents the amount of the product in the transaction indexed by s, i, p, t . The amount bought per product is computed directly from the data, since we observe the products that a firm buys through its transactions. On the other hand, we cannot observe the products that a firm *consumes* from their inventory; only the finished products that they supply to others. So, we need to learn the function mapping from products externally supplied to products internally consumed from the inventory. We estimate the total amount of product p consumed by firm i at time t as

$$\text{consume}(i, p, t) = \sum_{e(i,b,p_s,t) \in \mathcal{E}} \alpha_{p_s p} \cdot \text{amt}(i, b, p_s, t), \quad (2)$$

where $\alpha_{p_s p} \in \mathbb{R}_+$ is a learned attention weight representing how much of product p is needed to make one unit of the product supplied, p_s . In other words, each product *attends to* its parts. Finally, let $\mathbf{b}_i^{(t)}$ represent the vector over all products of amount bought by firm i at time t , and let $\mathbf{c}_i^{(t)}$ be defined analogously for consumption. Then the firm’s updated inventory is

$$\mathbf{x}_i^{(t+1)} = \max(0, \mathbf{x}_i^{(t)} + \mathbf{b}_i^{(t)} - \mathbf{c}_i^{(t)}). \quad (3)$$

²For simplicity, we assume in this work that there is one way to make each product, but future work may consider extensions, such as firm-specific product graphs or products that are substitutes for each other.

We take the elementwise max with 0 to ensure that the inventory stays non-negative, but we also penalize whenever consumption exceeds the current inventory amounts (see Eq. 6 below).

Attention weights. If the inventory module is standalone, then we directly learn the pairwise weights $\alpha_{p_1 p_2}$ for all product pairs p_1, p_2 . If the inventory module has access to product embeddings (e.g., from a GNN), we can use product embedding $\mathbf{z}_p \in \mathbb{R}^d$ to inform the attention weights as

$$\alpha_{p_1 p_2} = \text{ReLU}(\mathbf{z}_{p_1} \mathbf{W}_{\text{att}} \mathbf{z}_{p_2} + \nu_{p_1 p_2}), \quad (4)$$

where $\mathbf{W}_{\text{att}} \in \mathbb{R}^{d \times d}$ and $\nu_{p_1 p_2} \in \mathbb{R}$ are learned parameters, and we apply ReLU to ensure that the attention weights are non-negative. Compared to directly learning the attention weights, here we treat $\mathbf{z}_{p_1} \mathbf{W}_{\text{att}} \mathbf{z}_{p_2}$ as the base rate and $\nu_{p_1 p_2}$ as adjustments, which we encourage to be small in magnitude with L_2 regularization (6). By using the embeddings to form the base rate, instead of learning each pair independently, we can share information across product pairs, which is especially useful given sparse real-world data where we rarely observe most pairs.

Inventory loss. To train the inventory module, we introduce a special loss function. For a given firm i at time t , its inventory loss is

$$\ell_{\text{inv}}(i, t) = \lambda_{\text{debt}} \sum_{p \in [m]} \max(0, \text{consume}(i, p, t) - \mathbf{x}_i^{(t)}[p]) - \lambda_{\text{cons}} \sum_{p \in [m]} \text{consume}(i, p, t). \quad (5)$$

That is, we penalize inventory debt, i.e., whenever consumption exceeds the current inventory, but otherwise reward consumption. We penalize inventory debt since firms should not be able to consume products that they never received. Furthermore, penalizing inventory debt results in *sparse* attention weights, since for most firms, we do not observe it buying most products, so for any of those products that it does not buy, it would prefer to never consume those products since it would immediately go into inventory debt if so. On the other hand, we need the consumption reward in order to prevent trivial solutions. Without it, the model could learn $\alpha_{p_1, p_2} \approx 0$ for all product pairs, and it would never experience inventory debt. We use hyperparameters λ_{debt} and λ_{cons} to control the relative weight between penalizing inventory debt and rewarding consumption, and in practice, we find that choosing λ_{debt} around 25% larger than λ_{cons} works well (Table 4). All together, the inventory loss is

$$\ell_{\text{inv}}(t) = \frac{1}{n} \sum_{i \in [n]} \ell_{\text{inv}}(i, t) + \lambda_{L_2} \sqrt{\sum_{p_1, p_2 \in [m]} \nu_{p_1 p_2}^2}. \quad (6)$$

2.2.2 SC-TGN

The first GNN we explore is Temporal Graph Network (TGN) (Rossi et al., 2020), which is one of the most established GNNs for dynamic link prediction, outperforming other models in the Temporal Graph Benchmark (Huang et al., 2023). In our work, we have extended TGN to SC-TGN, by enabling it to (1) perform message passing over *hypergraphs*, since we represent each transaction as an edge between three nodes, (2) predict edge weights (i.e., transaction amounts) in addition to edge existence. We also modified TGN in other ways that improved performance; we document these changes in Appendix A.1. In SC-TGN, each node i has a time-varying memory $\mathbf{m}_i^{(t)}$. Each transaction $e(s, b, p, t)$ sends three messages: one each to the supplier s , buyer b , and product p . At the end of each timestep, each node aggregates the messages it received and updates its memory, using a recurrent neural network (RNN). Then, to produce node embedding $\mathbf{z}_i^{(t)}$, we apply a GNN to the node memories, so that nodes can also learn from their neighbors’ memories (this is useful for preventing staleness, if a node has not had a transaction in a while).

2.2.3 SC-GraphMixer

We also explore GraphMixer (Cong et al., 2023), a recent model that showed that temporal GNNs do not always need complicated architectures, such as RNNs or self-attention (both of which are used by TGN), and strong performance can sometimes be achieved with simpler models that only rely on multi-layer perceptrons (MLPs). We similarly extend GraphMixer to SC-GraphMixer, so that it can handle hypergraphs and predict edge weight in addition to edge existence (Appendix A.2). In SC-GraphMixer, each node’s embedding $\mathbf{z}_i^{(t)}$ is a concatenation of its node encoding and link encoding. The node encoding is simply a sum of the node’s features and mean-pooling over its 1-hop neighbors’ features. The link encoding summarizes the recent edges that the node participated in, by applying an MLP to the concatenated time encodings and features of the recent edges.

2.2.4 Decoder

Both models, SC-TGN and SC-GraphMixer, use the same decoder architecture, and we use the same architecture (although separate decoders) for predicting edge existence and edge weight. We model these as a two-step process: first, predicting whether an edge exists; second, conditioned on the edge existing, predicting its weight. The decoder is a two-layer MLP over the concatenation of the supplier firm’s, buyer firm’s, and product’s embeddings, producing $\hat{y} \in \mathbb{R}$:

$$\hat{y}(s, b, p, t) = \text{DEC}(\mathbf{z}_s^{(t)}, \mathbf{z}_b^{(t)}, \mathbf{z}_p^{(t)}) = \text{MLP}([\mathbf{z}_s^{(t)} | \mathbf{z}_b^{(t)} | \mathbf{z}_p^{(t)}]). \quad (7)$$

Real values are natural for both prediction tasks, since for edge existence, we apply a softmax over alternatives and use cross-entropy loss to evaluate the probability of the positive transaction compared to negative samples, and for edge weight, we apply log-scaling and standard scaling to the transaction amounts so negative predicted amounts are valid.

When the inventory module is attached, we may also allow it to inform edge prediction. To help with predicting edge existence, the inventory module *penalizes* impossible transactions, i.e., some (s, b, p, t) where the supplier s does not have enough parts to make product p :

$$\text{pen}(s, b, p, t) = - \sum_{p' \in [m]} \max(0, \alpha_{pp'} - \mathbf{x}_s^{(t)}[p']). \quad (8)$$

Then, our model’s new prediction for edge existence becomes the sum of the original \hat{y} in (7) and the penalty (8). To help with predicting edge weight, i.e., transaction amount, the inventory module computes a *cap* on the maximum amount of product p that supplier s could produce at this time:

$$\text{cap}(s, b, p, t) = \min_{p' \in [m]; \alpha_{pp'} > 0} \left\{ \frac{\mathbf{x}_s^{(t)}[p']}{\alpha_{pp'}} \right\}. \quad (9)$$

Then, our new predicted amount is the minimum of the original predicted amount (7) and the cap (after applying the same log-scaling and standard scaling to the cap that we did to all amounts). Thus, as shown in Figure 1b, the inventory module and GNN help each other, with the GNN’s embeddings informing the inventory module’s attention weights, and the inventory module’s penalties and caps affecting future edge prediction.

2.3 Model training and evaluation

Learning production functions. Our model does not have access to any production functions during training, but the goal is for the model to learn production functions via the inventory module and its specialized loss. For each product p , we have the set of its attention weights $\{\alpha_{pp_1}, \alpha_{pp_2}, \dots, \alpha_{pp_m}\}$, and we can compute the ranking over all products from highest to lowest weight. We compare this ranking to the product’s ground-truth parts, i.e., the parents of p in G_{prod} , and use average precision (17) to quantify performance. Then, we compute the mean average precision (MAP) over all products for which we have ground-truth parts. We have ground-truth parts for all products in our synthetic data (Section 3.2) and for scanning electron microscopes in real-world data (Section 3.1).

Edge existence and negative sampling. We perform negative sampling such that each positive transaction $e(s, b, p, t)$ is paired with a set of negative transactions that did not actually occur at time t . Following Temporal Graph Benchmark (Huang et al., 2023), we sample two types of hard negatives: first, randomly perturbing one of the three nodes; second, sampling a *historical* negative, meaning a transaction that appeared in training but not at time t . Compared to a uniform random negative, these negatives are far harder to distinguish from the positive transaction. For the perturbations, they match the positive transaction on two of the three nodes, requiring the model to make a distinction based on the third node. The historical negatives are even harder: this transaction *has* been observed before, but it does not occur at this timestep, requiring the model to learn time-varying properties of the graph. For each positive transaction, we sample 9 perturbation negatives and 9 historical negatives. To evaluate performance, we use mean reciprocal rank (MRR), which evaluates the rank of the positive transaction among the negatives (19). However, MRR is non-differentiable, so during training, we use softmax cross-entropy as a strong proxy loss for MRR (Bruch et al., 2019).

Edge weight. Since we model edge prediction as a two-stage process, we only predict edge weight (i.e., transaction amount) conditioned on the edge existing. Thus, training and test edge weight prediction is simple: we only consider the positive transactions and we compare the model’s predicted amount to the true amount using root mean squared error (RMSE) (20). Unlike MRR, RMSE is differentiable, so we also use it in the model loss during training.

3 Supply chains data

To evaluate our models, we collected two real-world datasets of supply chain transactions, and built a simulator, `SupplySim`, which can generate realistic supply chain data under varied settings. While we cannot release the real-world datasets, due to their proprietary nature, we carefully document our data sources and collection processes. Furthermore, we release `SupplySim` (which matches the real data on key characteristics) and the three synthetic datasets that we evaluate our models on in this work. We describe both data types here, with details in Appendix B and data statistics in Table 3.

3.1 Real-world supply chains data

We acquired transactions data from TradeSparq, a third-party data provider which aggregates data from authorized government sources (e.g., customs departments) across 60+ countries. Their data sources include bills of lading, receipts of reported transactions, and custom declarations. Each product being transacted is described with a Harmonized System (HS) code, where HS6 is an internationally recognized six digit number that describes products in terms of their chapters (first two digits), headings (next two digits), and subheadings (last two digits). For example, the HS code 840731 refers to the chapter 84 (chapter: Machinery), 07 (heading: Spark-ignition Reciprocating Piston Engines), and 31 (sub-heading: engines type not over 50CC cylinder capacity). Along with HS codes, the transactions data also includes the company name and ID of the supplier, the company name and ID of the buyer, timestamp of the transaction, cost in USD, and so on. Using the TradeSparq data (which we could only access via API calls, with costs per call), we constructed two supply chains datasets. For both datasets, we began by selecting specific HS codes that we were interested in, identifying their prominent suppliers, then using breadth-first-search to collect their neighbors upstream and downstream in the supply chain (see flowchart in Figure 3). This collection process allowed us to capture all interactions between firms within multiple tiers of the supply chain.

Automotive dataset (Tesla). This dataset focuses on electric vehicles (EV) and EV parts supplied by Tesla. We identified Tesla EV makers, their direct suppliers and buyers, and their suppliers’ suppliers, and included all transactions between these firms from January 1, 2019, to December 31, 2022.

Industrial equipment dataset (IED). This dataset focuses on microscopes along with other specialized analytical and inspection equipment and their manufacturers. We included makers of these products and their direct suppliers and buyers, and included all transactions between these firms in 2023. Compared to the Tesla dataset, this dataset is broader (i.e., more firms per layer) but shorter in time and depth (i.e., fewer layers). For this dataset, we have also estimated the ground-truth parts of microscopes in terms of their HS codes, which we use to test our inventory module’s ability to infer production functions from transactions.

3.2 Supply chains simulator, `SupplySim`

The TradeSparq data offers a rare opportunity to test models on real transaction-level data, but it also has shortcomings: the transactions are incomplete, most production functions are missing, and we cannot release the data. Thus, we design a simulator, `SupplySim`, that addresses these shortcomings and enables us to test the model under *controlled* settings (e.g., complete vs. incomplete transactions, stable supply vs. shocks). There are three stages to the simulator: (1) constructing the production graph, G_{prod} , (2) assigning products to suppliers and assigning suppliers to buyers, (3) generating time-varying transactions between firms. We ensure that our generated graphs match real-world supply chain networks on known characteristics, such as power law degree distributions.

Constructing the production graph, G_{prod} . Given the number of products, m , we partition the products into tiers and sample a 2-dimensional position for each product from $\text{Uniform}(0, 1)$. Then, for each tier, we assign the products in the tier to parts from the previous tier, with probability

| | SS-std | SS-shocks | SS-missing | IED |
|---------------------------|----------------------|----------------------|----------------------|----------------------|
| Random baseline | 0.124 (0.009) | 0.124 (0.009) | 0.124 (0.009) | 0.060 (0.002) |
| Temporal correlations | 0.745 | 0.653 | 0.706 | 0.128 |
| PMI | 0.602 | 0.602 | 0.606 | 0.175 |
| node2vec | 0.280 | 0.280 | 0.287 | 0.127 |
| Inventory module (direct) | 0.771 (0.005) | 0.770 (0.006) | 0.744 (0.006) | 0.143 (0.004) |
| Inventory module (emb) | 0.790 (0.005) | 0.778 (0.011) | 0.755 (0.007) | 0.262 (0.005) |

Table 1: Results for production learning, evaluated with mean average precision (MAP \uparrow). For the models with randomness, we report mean and standard deviation (in parentheses) over 10 seeds.

proportional to the inverse distance between their positions. For each part-product pair, we also sample u_{io} , the number of units of the part p_i needed to make one unit of the product p_o . The tier structure imitates tiers in real-world supply chains; for example, products at the first tier are raw materials, e.g., minerals, and products at the final tier are consumer products. The products’ positions capture the product type, e.g., its industry, and assigning parts based on positions reflects how parts should be similar to their products and naturally results in commonly co-occurring parts.

Constructing supplier-buyer relations. Given the number of firms, n , we also sample a 2-dimensional position from Uniform(0, 1) for each firm, and we restrict the firm to a subset of two consecutive tiers, meaning it can only produce products in those tiers. Then, for each product, we select its suppliers from the set of firms that are allowed to produce that product, again with probability proportional to inverse distance. Now, each firm has a set of products that it is supplying, which means, based on G_{prod} , we know which input parts it needs to buy. For each pair (b, p) , where firm b needs to buy product p , we assign it to a supplier of p with probability proportional to the number of buyers that the supplier already has. This assignment mechanism, known as preferential attachment (Newman, 2001), yields power law degree distributions, which are known to appear in real-world supply chain networks (Fujiwara and Aoyama, 2010; Zhao et al., 2019).

Generating transactions. We generate transactions based on the ARIO model, an agent-based model widely used in economics to simulate propagation over supply chains (Hallegatte, 2008; Inoue and Todo, 2019; Guan et al., 2020). At each timestep of the simulation, each firm completes as many of its incomplete orders as it can until it runs out of inventory. Each time it completes an order for k amount of output product p_o , it subtracts $k \cdot u_{io}$ of input product p_i from its inventory (i.e., we assume the production function \mathcal{F}_{p_o} is linear). At the end of the timestep, the firm places orders to its suppliers, based on what it needs to complete its remaining orders. Finally, the reported transactions are the completed orders in each timestep. The simulator also keeps track of the exogenous supply for products in the first tier, which do not require parts, and of exogenous demand for products in the final tier, which are only bought by consumers and not by other firms. By manipulating the exogenous supply, we can model shocks in the supply chain.

4 Experiments

We run experiments on the two real-world supply chain datasets and three synthetic datasets from SupplySim: a standard setting with high exogenous supply (“SS-std”), a setting with shocks to exogenous supply (“SS-shocks”), and a setting with missing transactions (“SS-missing”), where we sampled 20% of firms uniformly at random and dropped all transactions where they were buyer or supplier, reflecting firms that are missing from real-world supply chains data. In all experiments, we order the transactions chronologically and split them into train (the first 70%), validation (the following 15%), and test (the last 15%). Here we describe our results on these datasets, with additional details about the experimental set-up and supplemental results in Appendix C.

4.1 Learning production functions

We try three baselines, which each compute scores for output product p_o and potential input p_i :

1) Temporal correlations: we expect that inputs and outputs are temporally correlated, so this method computes the maximum correlation, with possible lags, between the buying timeseries of p_i and supplying timeseries of p_o , averaged over all firms that buy p_i and supply p_o .

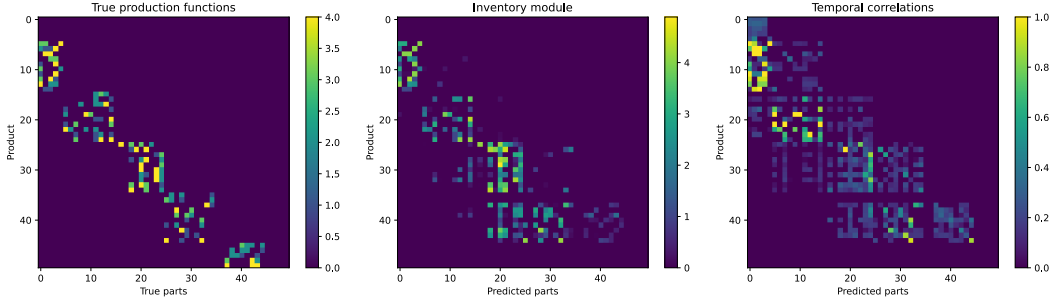


Figure 2: True production functions (left), predictions from inventory module (middle), predictions from temporal correlations (right), trained on SS-std.

2) Pointwise Mutual Information (PMI): we expect that input-output pairs appear with greater frequency in the firm-product graph,³ so this method computes the probability that a firm buys p_i and supplies p_o , divided by the product of their individual probabilities (26).

3) node2vec: we expect that inputs are close to outputs, so this method computes the cosine similarity of p_i and p_o 's node2vec embeddings, learned over the firm-product graph.

The three baselines capture the usefulness of temporal information, 1-hop neighbors in the graph, and the entire graph, respectively. In contrast, our inventory module captures both temporal and structural information. We try two versions of the inventory module, one that learns the attention weights directly and one that uses product embeddings, as described in (4). We also report a random baseline, which produces uniform random rankings of parts for each product.

We summarize the production learning results in Table 1. We find that the inventory module significantly outperforms the baselines, with especially large margins on the real-world data (IED) and in the synthetic data, when there are shocks in supply. In the standard synthetic data, when supply is plentiful, temporal correlations are a strong predictor since firms place orders for inputs, receive them promptly, then supply their own outputs shortly after. However, once there are shocks, the firm will receive inputs at different times, due to delays, and since they cannot produce their outputs until all inputs have arrived, the correlation in time of buying inputs and supplying outputs is seriously worsened. On the other hand, the inventory module is robust to such delays, since it does not rely on similarity in timeseries; simply that an input must go into the inventory *before* the output comes out. The inventory module is also remarkably robust to missing data: the MAP only drops by 3.5 points (4.4%) when we drop 20% of firms in the synthetic data. We also see that using product embeddings, instead of learning the attention weights directly, consistently helps the inventory module.

Figure 2 visualizes our results, showing that the inventory module effectively learns the true production functions. The block structure visible in all three subfigures reflects how our products were partitioned into tiers (products 0-4 in tier 0, 5-14 in tier 1, 15-24 in tier 2, and so on) and products in one tier served as viable parts for the next tier. The inventory module recovers the tier structure much more precisely, while temporal correlations show positive weights in larger blocks. The inventory module also learns attention weights of similar magnitude as the true production functions, while the temporal correlations are constrained between 0 and 1, and the other baselines are similarly not comparable to the true production functions on magnitude, only ranking. While only ranking matters for MAP, magnitude is essential if using the inventory module to inform edge prediction with penalties (8)-(9). Finally, in Figure 6, we show that our inventory module's loss function (6) is well-correlated with MAP, which is why it can effectively learn production functions without observing any of them.

4.2 Predicting future edges

For edge existence, where we seek to predict whether future transaction (s, b, p, t) exists, we compare our models to the following baselines:

³The firm-product graph is a static bipartite graph of firm and product nodes, where an edge between a firm and product indicates that the firm buys or supplies the product.

| | SS-std | SS-shocks | SS-missing | Tesla | IED |
|-------------------|----------------------|----------------------|----------------------|----------------------|----------------------|
| Edgebank (binary) | 0.174 | 0.173 | 0.175 | 0.131 | 0.164 |
| Edgebank (count) | 0.441 | 0.415 | 0.445 | 0.189 | 0.335 |
| Static | 0.439 (0.001) | 0.392 (0.002) | 0.442 (0.001) | 0.321 (0.001) | 0.358 (0.001) |
| Graph transformer | 0.431 (0.003) | 0.396 (0.024) | 0.428 (0.003) | 0.507 (0.020) | 0.613 (0.045) |
| SC-TGN | 0.522 (0.003) | 0.449 (0.004) | 0.494 (0.004) | 0.820 (0.007) | 0.842 (0.004) |
| SC-TGN+inv | 0.540 (0.003) | 0.461 (0.009) | 0.494 (0.004) | 0.818 (0.004) | 0.841 (0.008) |
| SC-GraphMixer | 0.453 (0.005) | 0.426 (0.004) | 0.446 (0.003) | 0.690 (0.027) | 0.791 (0.009) |
| SC-GraphMixer+inv | 0.497 (0.004) | 0.448 (0.004) | 0.446 (0.002) | 0.681 (0.014) | 0.791 (0.008) |
| Edgebank (avg) | 0.341 | 0.387 | 0.349 | 1.148 | 0.489 |
| Static | 0.343 (0.008) | 0.425 (0.019) | 0.374 (0.027) | 1.011 (0.007) | 0.504 (0.018) |
| Graph transformer | 0.340 (0.005) | 0.398 (0.025) | 0.361 (0.016) | 0.885 (0.024) | 0.425 (0.008) |
| SC-TGN | 0.303 (0.003) | 0.359 (0.007) | 0.313 (0.002) | 0.796 (0.012) | 0.428 (0.011) |
| SC-TGN+inv | 0.312 (0.003) | 0.370 (0.009) | 0.312 (0.002) | 0.801 (0.015) | 0.422 (0.011) |
| SC-GraphMixer | 0.318 (0.003) | 0.384 (0.005) | 0.330 (0.005) | 0.774 (0.077) | 0.457 (0.008) |
| SC-GraphMixer+inv | 0.320 (0.004) | 0.378 (0.005) | 0.328 (0.003) | 0.767 (0.054) | 0.454 (0.012) |

Table 2: Results for edge prediction. Top 8 rows are edge existence, evaluated with mean reciprocal rank (MRR \uparrow). Bottom 7 rows are edge weight (i.e., transaction amount), evaluated with root mean squared error (RMSE \downarrow). We report mean and standard deviation (in parentheses) over 10 seeds.

1) Edgebank: the “binary” version predicts 1 if $(s, b, p, *)$ appeared before in the train set; 0 otherwise. The “count” version predicts the number of times that $(s, b, p, *)$ appeared in the train set.

2) Static: learns a static vector to represent each node (no GNN).

3) Graph transformer: learns a static embedding to represent each node, using the UniMP model (Shi et al., 2021) which utilizes a graph transformer architecture and multi-head attention.

While Edgebank simply memorizes the train set, it serves as a strong baseline, as the Temporal Graph Benchmark (Huang et al., 2023) found that even the binary version outperformed some GNNs on dynamic link prediction. The latter two baselines test two types of static node embeddings, which allow us to isolate the benefit of dynamic node embeddings. For each of our models (SC-TGN and SC-GraphMixer), we try them alone and with the inventory module (+inv). For edge weight, we test the same set of methods, except for Edgebank, where we now predict the average amount for $(s, b, p, *)$ in the train set, or 0 (which is the mean amount, after standard scaling) if the triplet never appeared in train.

We summarize the edge prediction results in Table 2. First, we find that our models, SC-TGN and SC-GraphMixer, outperform the baselines on both tasks and all five datasets, by 11-62% on edge existence and 1-13% on edge weight. Second, we find that SC-TGN consistently outperforms SC-GraphMixer; we hypothesize this is because of SC-TGN’s sophisticated updating of node memories, while SC-GraphMixer only captures changes over time through its link encoder, which encodes the features and timestamps of the node’s recent edges, and its node encoder relies on the node’s static features (Appendix A.2). Supporting this hypothesis is the fact that the static methods perform poorly, demonstrating the need for TPGs to be represented with dynamic node embeddings. Since we find that SC-TGN outperforms SC-GraphMixer, we also compared SC-TGN to ablated versions: the original TGN, to test the value of our extensions (which we document in Appendix A.1), and to SC-TGN where the node memory is directly used as the embedding, instead of applying a GNN (UniMP in our case) to the memories. We find that the full SC-TGN outperforms both ablations substantially, by 34-45% and 53-100%, respectively (Table 5).

We also find in the synthetic data experiments, the setting with shocks is the hardest, resulting in lower MRRs and higher RMSEs across models. This demonstrates how shocks complicate prediction on TPGs, since shocks both delay firms’ abilities to complete their orders and limit them to producing smaller amounts, thus affecting both edge existence and edge weight. However, adding the inventory module significantly improves MRRs for both SC-TGN and SC-GraphMixer, on standard synthetic data and with shocks. In general, even though adding the inventory module introduces an additional loss so that we can learn production functions (16), we find that it does not hurt edge prediction performance, and in several cases, improves performance.

5 Related work

Many real-world systems can be represented as temporal graphs, such as transportation systems (Jiang and Luo, 2022), human mobility patterns (Chang et al., 2023), and biological networks (Prill et al., 2005). While most GNNs are designed for static graphs, in recent years, there has been growing interest in developing GNNs for temporal graphs, as noted by the Temporal Graph Benchmark (Huang et al., 2023) and surveys on temporal GNNs (Skarding et al., 2021; Longa et al., 2023). However, to the best of our knowledge, GNNs have not yet been designed to handle temporal production graphs (TPGs), as described in this work. Furthermore, only a handful of works have explored GNNs for supply chains: Aziz et al. (2021) and Kosasih and Brintrup (2022) use GNNs to predict hidden links between firms in the static supply chain network, and Wasi et al. (2024) provide a benchmark dataset for GNNs, consisting of a graph where nodes are products and edges represent relationships between products (e.g., same product group, same storage location). In contrast, we construct a dynamic supply chain network consisting of firm and product nodes, and our goals are to learn production functions and to forecast future transactions on this network.

Our work also has connections to temporal causal discovery (Nauta et al., 2019; Löwe et al., 2022; Assaad et al., 2022), where the goal is to learn a causal graph between variables based on their timeseries. Here, the variables are the products, but our setting is different since the timeseries appear as in-edges and out-edges embedded within the supply chain network, with each product having multiple timeseries (for different firms that buy and supply it). Our work is also related to inferring networks from node marginals (Kumar et al., 2015; Maystre and Grossglauser, 2017; Chang et al., 2024) and combining deep learning with domain-specific principles, a theme which appears in physics simulation (Wang et al., 2021) and epidemiological forecasting (Liu et al., 2024).

Within the supply chains domain, our work builds on prior literature that represents supply chains as networks (Fujiwara and Aoyama, 2010) and models the propagation of shocks over these networks (Acemoglu et al., 2012; Zhao et al., 2019; Li et al., 2020; Carvalho et al., 2021). Our work is unique in two key ways: first, much of the prior work relies on theoretical models and synthetic networks, and, even among empirical studies, the data used is typically industry-level or, at best, firm-level with static relations between firms (Carvalho and Tahbaz-Salehi, 2019). In contrast, we have access to *transaction*-level data, which reveals essential time-varying information. Second, integration of ML into supply chains has been limited, and only recently have researchers begun exploring the use of ML in supply chains, with calls for further exploration (Baryannis et al., 2019; Brintrup et al., 2020; Younis et al., 2022). Most prior models for modeling supply chain propagation are mechanistic (Hallegatte, 2008; Guan et al., 2020; Inoue and Todo, 2020; Li et al., 2021) and limited in their ability to even fit aggregate counts, such as country-level GDP (Inoue and Todo, 2019). In contrast, by combining mechanistic models with GNNs, we can forecast individual transactions with remarkable accuracy, while maintaining the interpretability of the inventory module. Our model can also be used for critical supply chain applications, such as demand forecasting (Seyedan and Mafakheri, 2020), early detection of risks (Sheffi, 2015), and inventory optimization (Vandeput, 2020).

6 Conclusion

In this work, we have formalized TPGs, with supply chain networks as a canonical example, and developed a new class of GNNs to handle them. Our models successfully achieve two essential objectives in this setting—inferring production functions and predicting future edges—while preexisting GNNs focused on the latter. Furthermore, we build a new simulator, SupplySim, to evaluate models under varied and controlled TPG settings, and release the simulator and synthetic datasets to encourage further research development. In future work, we hope to apply our model to TPGs in other domains, such as biological, and to develop theoretical results for our inventory module, such as establishing identifiability conditions and connecting it to causal inference.

Acknowledgements

S.C. was supported in part by an NSF Graduate Research Fellowship, the Meta PhD Fellowship, and NSF award CCF-1918940. J.L. was supported in part by NSF awards OAC-1835598, CCF-1918940, DMS-2327709, and Stanford Data Applications Initiative. From Hitachi, we are thankful to Arnab Chakrabarti for his continuous support.

References

- Acemoglu, D., Carvalho, V. M., Ozdaglar, A., and Tahbaz-Salehi, A. (2012). The network origins of aggregate fluctuations. *Econometrica*, 80(5):1977–2016.
- Aigner, D. J. and Chu, S. F. (1968). On estimating the industry production function. *The American Economic Review*, 58(4):826–839.
- Assaad, C. K., Devijver, E., and Gaussier, E. (2022). Survey and evaluation of causal discovery methods for time series. *Journal of Artificial Intelligence Research*, 73.
- Aziz, A., Kosasih, E. E., Griffiths, R.-R., and Brintrup, A. (2021). Data considerations in graph representation learning for supply chain networks. In *ICML 2021 Workshop on Machine Learning for Data*.
- Baryannis, G., Dani, S., and Antoniou, G. (2019). Predicting supply chain risks using machine learning: The trade-off between performance and interpretability. *Future Generation Computer Systems*, 101:993–1004.
- Baumgartner, T., Malik, Y., and Padhi, A. (2020). Reimagining industrial supply chains. *McKinsey & Company*.
- Brintrup, A., Pak, J., Ratiney, D., Pearce, T., Wichmann, P., Woodall, P., and McFarlane, D. (2020). Supply chain data analytics for predicting supplier disruptions: a case study in complex asset manufacturing. *International Journal of Production Research*, 58(11):3330–3341.
- Bruch, S., Wang, X., Bendersky, M., and Najork, M. (2019). An analysis of the softmax cross entropy loss for learning-to-rank with binary relevance. In *Proceedings of the 2019 ACM SIGIR International Conference on the Theory of Information Retrieval (ICTIR'19)*.
- Carvalho, V. M., Nirei, M., Saito, Y. U., and Tahbaz-Salehi, A. (2021). Supply chain disruptions: Evidence from the great east japan earthquake. *The Quarterly Journal of Economics*, 136(2):1255–1321.
- Carvalho, V. M. and Tahbaz-Salehi, A. (2019). Production networks: A primer. *Annual Review of Economics*, 11:635–663.
- Chang, S., Koehler, F., Qu, Z., Leskovec, J., and Ugander, J. (2024). Inferring dynamic networks from marginals with iterative proportional fitting. In *Proceedings of the 41st International Conference on Machine Learning (ICML'24)*.
- Chang, S., Vrabac, D., Leskovec, J., and Ugander, J. (2023). Estimating geographic spillover effects of covid-19 policies from large-scale mobility networks. In *Proceedings of the 37th AAAI Conference on Artificial Intelligence (AAAI'23)*.
- Coelli, T. J., Rao, D. S. P., O'Donnell, C. J., and Battese, G. E. (2005). *An Introduction to Efficiency and Productivity Analysis*. Springer Science & Business Media.
- Cong, W., Zhang, S., Kang, J., Yuan, B., Wu, H., Zhou, X., Tong, H., and Mahdavi, M. (2023). Do we really need complicated model architectures for temporal networks? In *Proceedings of the 11th International Conference on Learning Representations (ICLR'23)*.
- Fujiwara, Y. and Aoyama, H. (2010). Large-scale structure of a nation-wide production network. *The European Physical Journal B*, 77:565—580.
- Grover, A. and Leskovec, J. (2016). node2vec: Scalable feature learning for networks. In *Proceedings of the 22nd ACM SIGKDD International Conference on Knowledge Discovery and Data Mining (KDD'16)*.
- Guan, D., Wang, D., Hallegatte, S., Davis, S. J., Huo, J., Li, S., Bai, Y., Lei, T., Xue, Q., Coffman, D., Cheng, D., Chen, P., Liang, X., Xu, B., Lu, X., Wang, S., Hubacek, K., and Gong, P. (2020). Global supply-chain effects of covid-19 control measures. *Nature Human Behaviour*, 4:577–587.
- Hallegatte, S. (2008). An adaptive regional input-output model and its application to the assessment of the economic cost of katrina. *Risk Analysis*, 28(3):779–799.

- Huang, S., Poursafaei, F., Danovitch, J., Fey, M., Hu, W., Rossi, E., Leskovec, J., Bronstein, M., Rabusseau, G., and Rabbany, R. (2023). Temporal graph benchmark for machine learning on temporal graphs. In *Proceedings of the 37th Annual Conference on Neural Information Processing Systems (NeurIPS'23)*.
- Inoue, H. and Todo, Y. (2019). Firm-level propagation of shocks through supply-chain networks. *Nature Sustainability*, 2:841–847.
- Inoue, H. and Todo, Y. (2020). The propagation of economic impacts through supply chains: The case of a mega-city lockdown to prevent the spread of covid-19. *PLoS ONE*, 15(9).
- Jiang, W. and Luo, J. (2022). Graph neural network for traffic forecasting: A survey. *Expert Systems with Applications: An International Journal*, 207(C).
- Kazemi, S. M., Goel, R., Jain, K., Kobzyev, I., Sethi, A., Forsyth, P., and Poupart, P. (2020). Representation learning for dynamic graphs: A survey. *Journal of Machine Learning Research*, 21(70):1–73.
- Kosasih, E. E. and Brintrup, A. (2022). A machine learning approach for predicting hidden links in supply chain with graph neural networks. *International Journal of Production Research*, 60(17):5380–5393.
- Kumar, R., Tomkins, A., Vassilvitskii, S., and Vee, E. (2015). Inverting a steady-state. In *Proceedings of the 8th ACM International Conference on Web Search and Data Mining (WSDM'15)*.
- Li, Y., Chen, K., Collignon, S., and Ivanov, D. (2021). Ripple effect in the supply chain network: Forward and backward disruption propagation, network health and firm vulnerability. *European Journal of Operational Research*, 291:1117–1131.
- Li, Y., Zobel, C. W., Seref, O., and Chatfield, D. (2020). Network characteristics and supply chain resilience under conditions of risk propagation. *International Journal of Production Economics*, 223.
- Liu, Z., Wan, G., Prakash, B. A., Lau, M. S. Y., and Jin, W. (2024). A review of graph neural networks in epidemic modeling. In *arXiv*.
- Longa, A., Lachi, V., Santin, G., Bianchini, M., Lepri, B., Liò, P., Scarselli, F., and Passerin, A. (2023). Graph neural networks for temporal graphs: State of the art, open challenges, and opportunities. In *arXiv*.
- Löwe, S., Madras, D., Zemel, R., and Welling, M. (2022). Amortized causal discovery: Learning to infer causal graphs from time-series data. In *Proceedings of the 1st Conference on Causal Learning and Reasoning (CLear'22)*.
- Maystre, L. and Grossglauser, M. (2017). Choicerank: Identifying preferences from node traffic in networks. In *Proceedings of the 34th International Conference on Machine Learning (ICML'17)*.
- Nauta, M., Bucur, D., and Seifert, C. (2019). Causal discovery with attention-based convolutional neural networks. *Machine Learning and Knowledge Extraction*, 1(1):312–340.
- Newman, M. E. J. (2001). Clustering and preferential attachment in growing networks. *Physical Review E*, 64.
- Prill, R. J., Iglesias, P. A., and Levchenko, A. (2005). Dynamic properties of network motifs contribute to biological network organization. *PLoS Biology*, 3(11).
- Rossi, E., Chamberlain, B., Frasca, F., Eynard, D., Monti, F., and Bronstein, M. (2020). Temporal graph networks for deep learning on dynamic graphs. In *ICML 2020 Workshop on Graph Representation Learning*.
- Seyedan, M. and Mafakheri, F. (2020). Predictive big data analytics for supply chain demand forecasting: methods, applications, and research opportunities. *Journal of Big Data*, 7(53).
- Sheffi, Y. (2015). Preparing for disruptions through early detection. *MIT Sloan Management Review*, 57(1).

- Shi, Y., Huang, Z., Feng, S., Zhong, H., Wang, W., and Sun, Y. (2021). Masked label prediction: Unified message passing model for semi-supervised classification. In *Proceedings of the 13th International Joint Conference on Artificial Intelligence (IJCAI'21)*.
- Skarding, J., Gabrys, B., and Musial, K. (2021). Foundations and modeling of dynamic networks using dynamic graph neural networks: A survey. *IEEE Access*, 9:79143–79168.
- The White House (2021). Executive order on america’s supply chains. Available at <https://www.whitehouse.gov/briefing-room/presidential-actions/2021/02/24/executive-order-on-americas-supply-chains/>.
- Tolstikhin, I., Houlsby, N., Kolesnikov, A., Beyer, L., Zhai, X., Unterthiner, T., Yung, J., Steiner, A., Keysers, D., Uszkoreit, J., Lucic, M., and Dosovitskiy, A. (2021). Mlp-mixer: An all-mlp architecture for vision. In *Proceedings of the 35th Conference on Neural Information Processing Systems (NeurIPS'21)*.
- Vandeput, N. (2020). *Inventory Optimization: Models and Simulations*. Walter de Gruyter GmbH, Berlin, Germany.
- Wang, R., Walters, R., and Yu, R. (2021). Incorporating symmetry into deep dynamics models for improved generalization. In *Proceedings of the 9th International Conference on Learning Representations (ICLR'21)*.
- Wasi, A. T., Islam, M. S., and Akib, A. R. (2024). Supplygraph: A benchmark dataset for supply chain planning using graph neural networks. *arXiv*.
- Younis, H., Sundarakani, B., and Alsharairi, M. (2022). Applications of artificial intelligence and machine learning within supply chains: systematic review and future research directions. *Journal of Modelling in Management*.
- Zhao, K., Zuo, Z., and Blackhurst, J. V. (2019). Modelling supply chain adaptation for disruptions: An empirically grounded complex adaptive systems approach. *Journal of Operations Management*, 65(2):190–212.

Appendix

A Details about model

We provide additional details about our model architecture and evaluation framework here.

A.1 SC-TGN

Here we describe SC-TGN, our extended version of TGN (Rossi et al., 2020), in greater detail. Like TGN, our model consists of the following modules:

Memory. In SC-TGN, each node has a time-varying memory $\mathbf{m}_i^{(t)}$. The memory captures the node’s state, influenced by all of the transactions we have seen for this node up to this point. We initialize each node’s memory to a *learnable* vector $\mathbf{v}_i^{(0)}$. The node’s memory is updated each time the node participates in a transaction.

Message function. Each transaction, $e(s, b, p, t)$, sends a message to the three participating nodes: the supplier firm s , buyer firm b , and product p . Following the original work, we represent the raw message msg_e as the concatenation of the nodes’ memories and a time encoding:

$$\text{msg}_e = [\mathbf{m}_s^{(t)} | \mathbf{m}_b^{(t)} | \mathbf{m}_p^{(t)} | \text{enc}(t)], \quad (10)$$

where $\text{enc}(t)$ is a temporal encoding of time t , implemented as a simple linear layer. Then, the message to the supplier is $M_s(\text{msg}_e)$, where M_s is a supplier-specific message encoder, implemented as a linear layer followed by a ReLU activation. M_b and M_p are buyer-specific and product-specific message encoders, respectively, with the same architecture as M_s .

Memory updater. First, for each firm i , we aggregate over the messages that it received at time t to produce $\bar{msg}_i^{(t)}$. Following the original work, we simply take the mean over messages. Then, we update node i 's memory with its aggregated message, using a recurrent neural network:

$$\mathbf{m}_i^{(t+1)} = RNN(\mathbf{m}_i^{(t)}, \bar{msg}_i^{(t)}). \quad (11)$$

Embedding. Finally, the embedding module produces an embedding $\mathbf{z}_i^{(t)}$ of node i at time t . Following the original work, we explore both an ‘‘ID’’ embedding, where the embedding is simply the node’s memory, and embeddings that are constructed by applying a GNN to the memories. For the GNN, we use the UniMP model (Shi et al., 2021), which is the model used in the TGN implementation by Temporal Graph Benchmark (Huang et al., 2023). UniMP is a graph transformer architecture with multi-head attention; we refer the reader to the original text for details. The advantage of the GNN-based embedding over the ID embedding is that the GNN allows the node’s embedding to adapt over time, even if the node itself has not been involved in a transaction in a while, thus avoiding the memory staleness problem (Kazemi et al., 2020). In Table 5, we show that using a GNN to construct node embeddings from the node memories, instead of directly using the node memories, greatly improves performance of SC-TGN.

New elements in SC-TGN. SC-TGN extends TGN in the following ways:

- **Hyperedges.** To adapt TGN to handle hyperedges, we modify the message function so that it sends a message to three nodes, instead of two nodes. To capture the nodes’ varying roles within each hyperedge (supplier, buyer, product), we also use separate message encoders M_s , M_b , and M_p , respectively. We also modified the decoder to predict relationships between three nodes instead of two nodes.
- **Predicting edge weight.** The original TGN only predicts edge existence, with a decoder that produces the probability of an edge existing between two nodes. Our model has two decoders: one to predict the probability of a transaction existing and, conditioned on a transaction existing, one to predict the amount of the transaction (i.e., edge weight).
- **Update penalty.** We found it useful to regularize the memories over time, so that the memory update (11) was encouraged to be small.

$$\ell_{\text{update}} = \frac{\lambda_{\text{update}}}{m+n} \sum_{i \in [m+n]} \|\mathbf{m}_i^{(t+1)} - \mathbf{m}_i^{(t)}\|_2. \quad (12)$$

- **Learnable initial memory.** We initialize the node’s memory to a learnable vector $\mathbf{v}_i^{(0)}$, instead of initializing all new nodes to the zero vector, which is what was done in the original TGN. Making the initial memory learnable allows the model to learn representations for nodes even before they have participated in any transactions.
- **Training following the negative sampling scheme.** In the original paper, the authors train TGN with only perturbation negatives and not historical negatives, but they test TGN on both kinds of negatives. We found that test performance increased substantially (+10 or more points in MRR) if the model could be also be trained on historical negatives.

A.2 SC-GraphMixer

Here we describe SC-GraphMixer, our extended version of GraphMixer (Cong et al., 2023), in greater detail. Like GraphMixer, our model consists of a link encoder and a node encoder:

Link encoder. The purpose of the link encoder is to capture information from recent links associated with the node.

- **Time encoding.** Given a timestep t , GraphMixer encodes the timestep by projecting it to a d -dimensional vector. The time-encoding function utilizes features $\omega = \{\alpha^{-(d'-1)/\beta}\}_{d'=1}^d$, where α and β are predefined hyperparameters, and projects t to $\cos(t \times \omega) \in [-1, +1]$.
- **To represent a given node i at time t ,** GraphMixer constructs the matrix $\mathbf{T}_i(t)$. Each row of this matrix corresponds to a recent link of node i 's, where the link is represented as the

concatenation of $\cos((t-t_e) \times \omega)$, where t_e is the timestep of the link, and the link’s features (in our case, the transaction amount). Encoding $t-t_e$ instead of t_e itself captures how recent the link was, and thus how much influence it should have over the current timestep.

- Then, GraphMixer applies a 1-layer MLP-mixer (Tolstikhin et al., 2021) to $\mathbf{T}_i(t)$:

$$\mathbf{H}_{\text{token}} = \mathbf{T}_i(t) + \mathbf{W}_{\text{token}}^{(2)} \text{GeLU}(\mathbf{W}_{\text{token}}^{(1)} \text{LayerNorm}(\mathbf{T}_i(t))) \quad (13)$$

$$\mathbf{H}_{\text{channel}} = \mathbf{H}_{\text{token}} + \text{GeLU}(\text{LayerNorm}(\mathbf{H}_{\text{token}}) \mathbf{W}_{\text{channel}}^{(1)}) \mathbf{W}_{\text{channel}}^{(2)}. \quad (14)$$

Finally, node i ’s link encoding at t , $\mathbf{t}_i(t)$, is the mean of $\mathbf{H}_{\text{channel}}$.

Node encoder. The purpose of the node encoder is to capture the node’s identity and its features, along with its neighbors’ features. To represent a given node i at time t , its node encoding, $\mathbf{s}_i(t)$, is

$$\mathbf{s}_i(t) = \mathbf{x}_i^{\text{node}} + \frac{1}{|\mathcal{N}(i; t-T, t)|} \sum_{j \in \mathcal{N}(i; t-T, t)} \mathbf{x}_j^{\text{node}}, \quad (15)$$

i.e., the sum of the node’s own features and the mean of the node’s neighbors’ features, where neighbors from time $t-T$ to t are included and T is a predefined hyperparameter.

Finally, GraphMixer’s node embedding of node i at time t is the concatenation of its node encoding and link encoding: $\mathbf{z}_i^{(t)} = [\mathbf{s}_i(t) | \mathbf{t}_i(t)]$.

New elements in SC-GraphMixer. SC-GraphMixer extends GraphMixer in the following ways:

- Hyperedges. To adapt GraphMixer to handle hyperedges, we compute both link and node embeddings for all three nodes instead of two nodes, and the input to the decoder is the concatenation of their three embeddings (7). For a product node, its recent links involve all recent transactions that it was involved in. For a firm node, its recent links involve all recent transactions where it was the supplier or the buyer. As in GraphMixer, the time encoding encodes the difference in time between when the transaction occurred and the current timestep.
- Learnable node features. The original GraphMixer treats node features as per-node fixed input to models. Inspired by the memory module of TGN, we introduced *learnable* node feature $\mathbf{x}_i^{\text{node}}$ for each node, when the dataset does not provide raw node features. The node features are randomly initialized and optimized as model parameters. Introducing learnable node features also means that the static node embedding is a strictly nested version of SC-GraphMixer, making it a proper ablation of both of our models.
- Predicting edge weight in addition to edge existence, as described above for SC-TGN.
- Training following the negative sampling scheme, as described above for SC-TGN.

A.3 Penalties and caps from inventory module

As described in the main text, when our inventory module is combined with a GNN, such as SC-TGN or SC-GraphMixer, we can optionally use the inventory module to help with predicting future edges, in addition to its primary purpose, which is to learn production functions. To help with predicting edge existence, the inventory module *penalizes* impossible transactions, as described in (8), and adds its penalty to the original prediction \hat{y} . To help with predicting edge weight, the inventory module computes a cap, i.e., the maximum amount possible in the transaction, as described in (9), and takes the minimum of its cap and \hat{y} . Note that, if the inventory module’s attention weights match the ground-truth production functions *and* the inventories reflect what the firm truly has at the time of the transaction, these penalties and caps can only help, not hurt, the prediction. This is because the penalty (8) will always be 0 for a true transaction while it can be negative for a false transaction, so adding the penalties can only help. Similarly, the amount cap (9) is guaranteed to be greater than or equal to the true transacted amount, so taking the minimum of the cap and the original predicted amount can also only help.

However, even if the learned attention weights match the ground-truth production functions closely, it is not guaranteed that the inventory reflects what each firm truly has at the time of the transaction. One minor case that we see of this is that the inventory is only updated up to time t , but the current batch

could include transactions at time $t + 1$ or later; thus, we only apply penalties or caps to transactions in time t , since at time $t + 1$ and later, the inventory will look different. A more serious case is when we are systematically missing transactions in the dataset, so as a result, we are underestimating the number of products that each firm has in its inventory, so penalties are too large and caps are too low. We investigate this issue in Appendix C.2 and show that, when some firms are missing from the synthetic data, the penalties and caps indeed hurt edge prediction performance, even if the attention weights are perfectly learned (we set them to the ground-truth production functions). So, it is preferable not to use the penalties and caps in those settings. In future work, it would be useful to explore how to make the inventory module more robust to missing data, so that we do not underestimate the number of products in the firms’ inventories even when transactions are missing. For example, some smoothing could be applied such that when we observe a firm buying product p , we also add a bit of p' to its inventory, where p' is a “similar” product, where similarity could be defined based on co-buying patterns.

A.4 Model training and evaluation

In summary, our model loss consists of four components,

$$\mathcal{L} = \ell_{\text{exist}} + \ell_{\text{weight}} + \ell_{\text{inv}} + \ell_{\text{update}}, \quad (16)$$

which correspond to the softmax cross-entropy loss from predicting edge existence; RMSE loss from predicting edge weight (20); the inventory loss (6); and an update loss that regularizes how much the node memories change between consecutive timesteps (12). Aside from ℓ_{exist} , each of the other losses has hyperparameters that control their relative weight. In Table 4, we document the hyperparameters we used in our experiments.

Learning production functions. We use mean average precision (MAP) to evaluate how well the inventory module learned the ground-truth production functions. Let \mathcal{P}_{p_o} represent the ground-truth set of parts for product p_o , let $\alpha_{p_o} = \{\alpha_{p_o p_1}, \alpha_{p_o p_2}, \dots, \alpha_{p_o p_m}\}$ represent the inventory module’s learned attention weights for p_o , and let $\text{pos}(\alpha_{p_o}, k)$ represent the product at rank k in α_{p_o} . We define average precision as

$$\text{AvePrec}(p_o) = \frac{1}{|\mathcal{P}_{p_o}|} \sum_{k=1}^m \text{Prec@K}(\alpha_{p_o}, \mathcal{P}_{p_o}, k) \cdot \mathbb{1}[\text{pos}(\alpha_{p_o}, k) \in \mathcal{P}_{p_o}] \quad (17)$$

$$\text{Prec@K}(\alpha, \mathcal{P}, k) = \frac{1}{k} \sum_{k'=1}^k \mathbb{1}[\text{pos}(\alpha, k') \in \mathcal{P}]. \quad (18)$$

In other words, average precision takes the average of Precision@K over all ranks k where there is a relevant item. Average precision and Precision@K are both common metrics in information retrieval, but we prefer average precision here since it can account for varying numbers of relevant items over queries, which applies to our setting since the size of \mathcal{P}_{p_o} varies across products.

Predicting edge existence. As described in the main text, we sample two types of negatives, perturbation negatives and historical negatives, to accompany each positive transaction. Temporal Graph Benchmark (Huang et al., 2023) also samples both types of negatives, although we modify the procedure slightly for hyperedges. For a positive transaction $e(s, b, p, t)$, we have three types of perturbation negatives: $e(s', b, p, t)$, where a random supplier is sampled; $e(s, b', p, t)$, where a random buyer is sampled; and $e(s, b, p', t)$, where a random product is sampled. A historical negative is a transaction $e(s', b', p', t)$ such that s', b', p' appeared in the train set, but not at time t . To make historical negatives even harder, we sample historical negatives proportionally to their count in the train set. For both types of negatives, we ensure that the sampled negative did not actually occur at time t . We sample 9 negatives following the perturbation procedure (with 3 of each type) and 9 negatives following the historical procedure. It is possible, though, that more than 9 negatives are historical (if the perturbation procedure results in a historical negative) or more than 9 negatives are perturbations (if a historical negative happens to be a one-node perturbation).

We use mean reciprocal rank (MRR) to evaluate performance for predicting edge existence. For each positive transaction e and its corresponding set of negatives \mathcal{N}_e in batch B , MRR quantifies the

| Attribute Counts | SS-std | Tesla | IED |
|------------------|--------|---------|---------|
| # Product Nodes | 50 | 2,690 | 3,029 |
| # Firms Nodes | 119 | 11,628 | 2,583 |
| # Transactions | 71646 | 581,002 | 279,712 |
| Timespan (Days) | 198 | 1683 | 359 |

Table 3: Dataset statistics.

position of the positive transaction among the negative samples:

$$MRR = \frac{1}{|B|} \sum_{e \in B} \left(\frac{\sum_{n \in \mathcal{N}_e} \mathbb{1}[\hat{y}_n < \hat{y}_e] + \sum_{n \in \mathcal{N}_e} \mathbb{1}[\hat{y}_n \leq \hat{y}_e]}{2} + 1 \right)^{-1}. \quad (19)$$

Following the Temporal Graph Benchmark (Huang et al., 2023), we compute an “optimistic” MRR where we tie-break in favor of the positive transaction and a “pessimistic” MRR where we tie-break in favor of the negative transactions, and take the average of the two. We refer to 0.1 as the random baseline, since we sample 18 negatives in total and, if all transactions received the same score, then the MRR would be $((0 + 18)/2 + 1)^{-1} = 0.1$. Similarly, if we assigned uniform random scores to all 19 alternatives, the expected rank of the positive is 10 (9 negatives before and 9 negatives after), so the reciprocal is 0.1.

Predicting edge weight. We preprocess transaction amounts by applying log-scaling then standard scaling, where we subtract the mean and divide by the standard deviation, so that amounts now have zero mean and variance of 1. We use the scaled amount as an edge feature, to stabilize training, and as a prediction target, to make RMSE comparable across datasets. However, note that we use the raw amount to update the inventory module, as required in (1)-(2). Then, we compare the predicted amount \hat{y} to the true amount, y , using root mean squared error:

$$RMSE = \sqrt{\frac{1}{|B|} \sum_{e \in B} (amt(e) - \hat{y}_e)^2}. \quad (20)$$

Since RMSE is differentiable, we use it both as the training loss and evaluation metric.

B Supply chains data

B.1 Real-world supply chains data

For our experiments, we constructed two large-scale, real-world supply chain datasets by compiling data from TradeSparq, a third-party data provider. We rely on a wide variety of data sources from authorized government sources across over 60 countries, including authorities like the Automated Manifest System, operated by US Customs and Border Protection, and other government customs departments. The data appear in the form of bills of lading (BoL), receipts of reported transactions, and custom declarations. Each transaction includes information such as data source, buyer title, supplier title, cost of reported transaction, product (in terms of HS code and description), import and export country, amount (weight and quantity unit), among other columns.

We have access to the data through an API, which allows us to make queries with associated costs. Due to these costs, we cannot reconstruct the entire supply chain network, but we focus on certain products and grow the network outwards via a breadth-first-search-like process. The construction begins by selecting product-specific HS codes and identifying prominent Tier-0 supplier firms involved in high-volume trading. The process captures all transactions from Tier-0 suppliers, then aggregates their group companies to identify Tier-1 suppliers, recording all corresponding transactions. This method is repeated to determine Tier-2 suppliers by analyzing the group companies of Tier-1 firms. All transactions between Tier-1 and Tier-2 firms are also collected. This systematic approach ensures a thorough mapping of supplier interactions up to Tier-2, providing detailed insights into the supply chain network. We illustrate our process as a flowchart in Figure 3.

Automotive dataset. Following this process, we constructed real-world automotive dataset within the Tesla, Inc. group companies involved in the electric vehicle (EV) and EV parts supply chain.

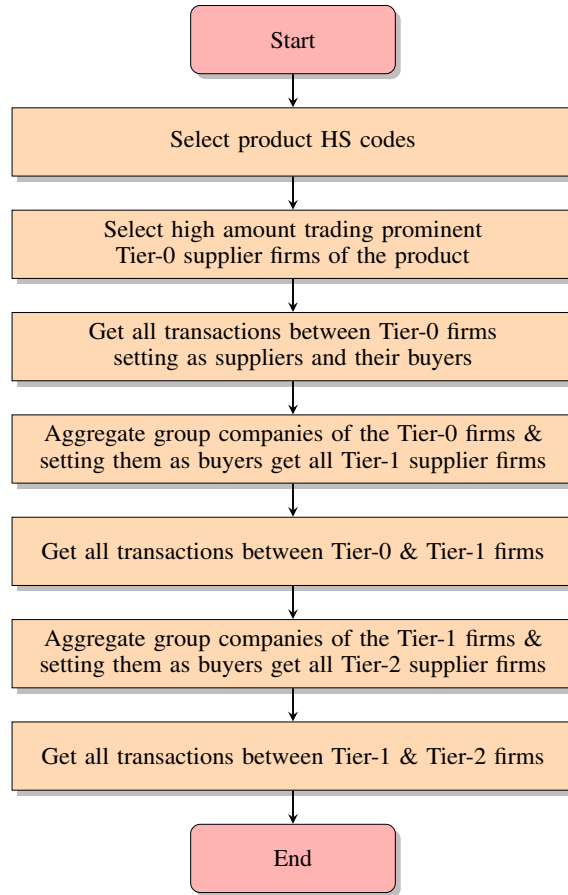


Figure 3: Overview of supply chain network data construction process.

The analysis covered transactions from January 1, 2019, to December 31, 2022. This process started by identifying Tesla EV maker firms and capturing all their transactions with Tier-1 suppliers, i.e. Tesla’s direct suppliers. Subsequently, Tier-1 suppliers were identified by aggregating Tier-1 firm groups and analyzing their transactions with Tier-2 supplier firms. This structured approach provided a comprehensive mapping of Tesla’s supply chain interactions, offering detailed insights into the dynamics and dependencies within their EV supply chain network.

Industrial equipment dataset. This dataset focuses on microscopes along with other specialized analytical and inspection equipment and their manufacturers. Spanning the years 2022 to 2023, the dataset covers approximately 630 makers. The process began with identifying Tier-0 suppliers associated with these specialized products and capturing all relevant transactions with their buyers. Further deep-tiers were constructed by aggregating transactions at Tier-1 and Tier-2 supplier levels, providing a detailed insight into the supply chain dynamics and the extensive network of suppliers involved in the production of these critical industrial tools. To construct the bill of material (BoM) for microscopes, we make use of an extensive survey of direct suppliers, inquiring about their products and their own suppliers. This survey, conducted in Japanese, required translating each supplied part name from Japanese to English. We then mapped these part names to HS codes using the HTS standard and manually verified the mappings. We successfully mapped and verified 87% of parts to HS codes, due to challenges posed by difficult and miscellaneous part names. Of the mapped parts, we could find 75% parts within our constructed supply chain. Consequently, we were able to construct 65% of the BoM for microscopes, which we then used to evaluate our inventory module.

Limitations of real-world supply chains data. TradeSparq data provides a rare opportunity to access transaction-level information, while most supply chain studies are done on much more aggregated data (e.g., imports and exports aggregated over country) or, at best, static firm-level

networks, without time-varying transactions (Inoue and Todo, 2019; Carvalho and Tahbaz-Salehi, 2019; Guan et al., 2020). However, there are still limitations of the real-world data, which motivate the need for synthetic data. We list some of these limitations below:

- Missing transactions. While TradeSparq covers 60+ countries, many transactions are also missing, especially domestic transactions that would not be reported in customs. Some companies may also deliberately obscure or omit details of their sensitive transactions in publicly available data to protect their business interests.
- Missing production functions. For most firms and products, we are missing their true production functions, which limits our ability to evaluate our inventory module.
- Proprietary data. Since the TradeSparq data is proprietary, we are not allowed to release it.
- Incomplete records. Essential fields such as transaction suppliers, quantities, and amounts may be missing, making it difficult to construct a complete picture of the transaction depending on the reporting country authority.
- Duplicate entries can arise from multiple sources reporting the same transaction.
- Transactions are reported at different times than actual production dates.
- Due to logistic constraints, multiple parts or products may be reported together.

B.2 Details about SupplySim

To address the limitations of real-world supply chains data, we build a simulator, SupplySim, which offers the following benefits:

- We can test the model under complete data settings, where all transactions are observed and all necessary data per transaction is provided. This allows us to disentangle model performance from data quality.
- We can also test how model performance changes as data quality changes, controlling how and to what extent it changes, such as dropping 20% of firms at random.
- We can generate any number of shocks, of varying size and source, and test the model’s ability to predict how transactions change under the shocks. In real data, large shocks are rare and confounded by many other contemporaneous factors so it is difficult to isolate their effect (e.g., shocks during the COVID-19 pandemic).
- We have production functions for all products, which enables us to evaluate the inventory module, and we can, again, vary the data settings to test how robust the inventory module’s performance is to missing data.
- Unlike the real-world data, we can release SupplySim and our generated synthetic data, improving the reproducibility and transparency of our research, along with encouraging future research in this domain.

Thus, SupplySim addresses all the limitations of real-world supply chains data, at the cost of being synthetic, instead of real-world, data. To mitigate this cost, we develop SupplySim to be as realistic as possible: for example, we ensure that the generated networks match real-world networks on key characteristics, such as degree distribution and clustering, and we use a realistic agent-based model from economics to generate time-varying transactions over the network.

As described in the main text, our simulator progresses in three steps: (1) constructing the production graph, G_{prod} , which describes static product-part relations, (2) assigning products to supplier firms and assigning supplier firms to buyer firms, which are also static relations, (3) generating time-varying transactions between firms.

B.2.1 Static graphs

Constructing the production graph, G_{prod} . First, we define the number of exogenous products n_{exog} , number of consumer products n_{consumer} , number of products per inner tier n_{tier} , and number of inner tiers T . Then, the products are assigned to tiers as follows:

- Tier 0: product 0 to product $n_{\text{exog}} - 1$,

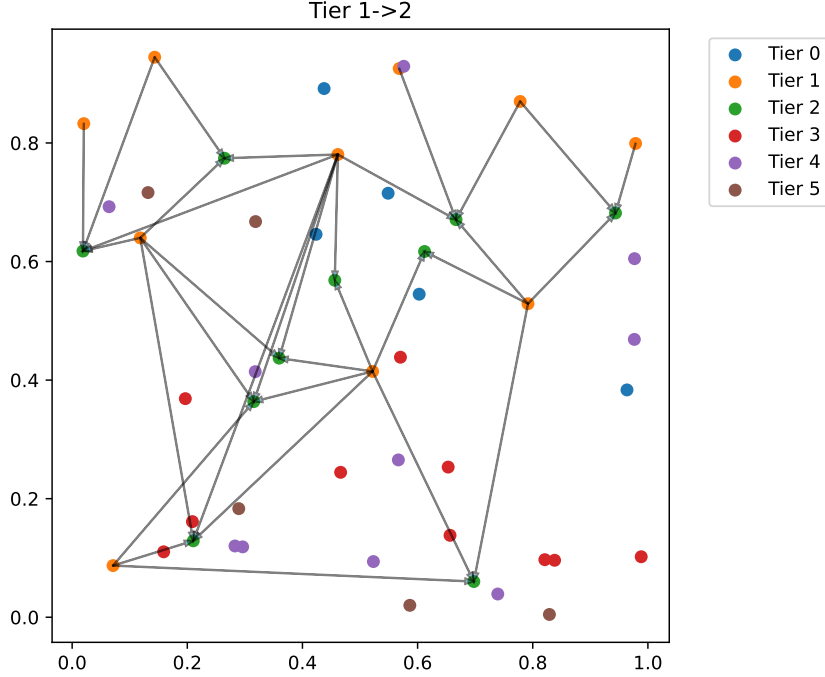


Figure 4: Visualizing products in our synthetic datasets. Each point represents the position of one of the 50 products, and points are color-coded by the product’s tier. We also denote part-product relations between Tier 1 and Tier 2 products, where an arrow from product p_1 to product p_2 means that p_1 is required to make p_2 . For each product, we sample its number of parts from $\{1, 2, 3, 4\}$ uniformly, then assign its parts to the closest products in the previous tier, resulting in commonly co-occurring parts.

- Tier 1: product n_{exog} to product $n_{\text{exog}} + n_{\text{tier}} - 1$,
- Tier 2: product $n_{\text{exog}} + n_{\text{tier}}$ to product $n_{\text{exog}} + 2 \cdot n_{\text{tier}} - 1$,
- ...
- Tier T : product $n_{\text{exog}} + (T - 1) \cdot n_{\text{tier}}$ to product $n_{\text{exog}} + T \cdot n_{\text{tier}} - 1$,
- Tier $T + 1$: product $n_{\text{exog}} + T \cdot n_{\text{tier}}$ to product $n_{\text{exog}} + T \cdot n_{\text{tier}} + n_{\text{consumer}} - 1$.

Thus, there are $n_{\text{exog}} + T \cdot n_{\text{tier}} + n_{\text{consumer}}$ products and $T + 2$ tiers overall. In our experiments, we use $n_{\text{exog}} = 5$, $n_{\text{consumer}} = 5$, $n_{\text{tier}} = 10$, and $T = 4$, resulting in 50 products. We also sample a 2-dimensional position from $\text{Uniform}(0, 1)$ for each product.

For each product, we sample its number of parts uniformly at random from a predefined range (we use 2 to 4, inclusive). Then, we select parts for the product, where the viable parts come from the previous tier. We assign the products to parts based on the distance between their positions, so that parts closer to the products are likelier to be chosen, with the probability proportional to $d^{-\gamma}$, where d is their distance. In our experiments, we deterministically assign products to their closest parts for simplicity, which is essentially equivalent to choosing an extreme γ , but it would be straightforward to introduce more randomness in the selection. In Figure 4, we visualize our products’ positions and the part-product relations between Tier 1 and Tier 2, demonstrating how this assignment procedure results in commonly co-occurring parts, while every product still has a unique set of parts. Commonly co-occurring parts are realistic, such as nails and bolts, and they create possible “similar” parts that can be learned by GNNs. For each pair of input part p_i and output product p_o , we also sample u_{i_o} uniformly at random (we use 1 to 4, inclusive), where u_{i_o} is the number of units of the part p_i needed to make one unit of the product p_o .

Constructing supplier-buyer relations. Now, we define the number of firms per “group”, n_{group} , where each group is assigned a set of n_{consec} consecutive tiers, such that the firms in the group are only allowed to supply products in this set of tiers. We define groups and tier sets as follows:

- Group 0: Tier 0 to Tier $n_{\text{consec}} - 1$,
- Group 1: Tier 1 to Tier n_{consec} ,
- Group 2: Tier 2 to Tier $n_{\text{consec}} + 1$,
- ...
- Group $T - n_{\text{consec}} + 2$: Tier $T - n_{\text{consec}} + 2$ to Tier $T + 1$.

In our experiments, we use $n_{\text{group}} = 30$ and $n_{\text{consec}} = 2$, resulting in 120 firms overall. For each firm, we also sample a 2-dimensional position from Uniform(0, 1).

Then, for each product, we sample its number of suppliers uniformly at random from a predefined range (we use 4 to 8, inclusive). Its set of viable supplier firms are the firms within the groups that supply products in this product’s tier. For example, in our experiments, a product at Tier 2 can be supplied by firms in Groups 1 and 2 (so 60 firms). Similar to how we assign parts to products, we assign suppliers to products based on the closest distances between the product and firm’s positions. Our procedure for assigning suppliers to products, where we restrict firms to consecutive tiers, results in more realistic supply chain graphs, since firms tend to specialize and we would not expect the same firm to produce products at very different tiers. Furthermore, by restricting firms to tiers and choosing suppliers based on closest distances, we also result in firms that supply similar sets of products, which is another form of similarity that can be captured in GNN representations.

Based on the assignment of suppliers to products, and the existing production graph G_{prod} , we can now determine which input products each firm needs to buy in order to make the products it supplies. We iterate through pairs (b, p) , where firm b needs to buy product p , and select a supplier firm s from all suppliers of p , with probability proportional to s ’s current number of buyers. This assignment mechanism, known as preferential attachment (Newman, 2001), reflects a rich-get-richer dynamic that results in power law degree distributions, which are known to appear in real-world supply chain networks (Fujiwara and Aoyama, 2010; Inoue and Todo, 2019; Zhao et al., 2019). Real-world firm-firm networks are also reported to have disassortativity (negative correlation between the degrees of connected nodes) and low clustering, which we also observe in our generated firm-firm networks: the degree assortativity is -0.253 and average clustering coefficient is 0.246, which is similar to the average clustering coefficient of 0.179 reported in Zhao et al. (2019).

B.2.2 Generating time-varying transactions

Now, given the static graphs, we want to generate time-varying transactions between firms. We base our simulation model on the ARIIO model, an agent-based model widely used in economics to simulate propagation over supply chains (Hallegatte, 2008; Inoue and Todo, 2019; Guan et al., 2020). At any point in the simulation, we keep track of each firm’s inventory $\mathbf{x}_i^{(t)}$; all incomplete orders $\mathcal{I}^{(t)}$, where an order is defined as $o(b, s, p, k)$, from buyer firm b to supplier firm s for k amount of product p ; and all orders that were newly completed at time t , $\mathcal{C}^{(t)}$. Then, at each timestep t , we iterate through firms, with each firm f taking the following actions.

- **New supply:** first, the firm adds its newly received products to its inventory, based on completed orders in $\mathcal{C}^{(t-1)}$ where it was the buyer. So, the firm is only allowed to use products from orders completed at time $t - 1$ at time t or later.
- **Production:** then, the firm goes through its incomplete orders and tries to complete as many as it can before it runs out of inventory. Each time the firm completes an order $o(b, f, p, k)$, it adds that order to $\mathcal{C}^{(t)}$, removes it from $\mathcal{I}^{(t)}$, and subtracts $u_{p_i p} \cdot k$ of input product p_i from its inventory, for all inputs p_i of product p . The firm goes through its incomplete orders from oldest to latest, and stops when $u_{p_i p} \cdot k$ exceeds what it has in its inventory. Thus, orders are completed first-in-first-out. This is a reasonable principle, since earlier orders should be completed earlier, but extensions could include prioritization or trying smaller, later orders after larger, earlier orders are no longer feasible.

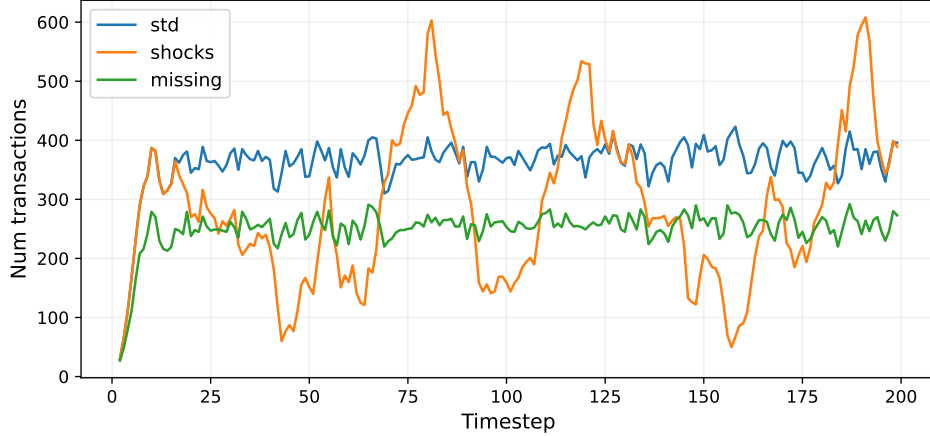


Figure 5: Visualizing the number of transactions per timestep, over the three synthetic datasets: SS-std, SS-shocks, and SS-missing.

- **New demand:** finally, the firm places new orders to its suppliers. First, for each input product p_i , it calculates the necessary amount $k_{f,p_i}^{(t)}$ as the amount it would need to complete all of its own incomplete orders minus the amount that is already pending in its incomplete orders to its suppliers:

$$k_{f,p_i}^{(t)} = \sum_{(b,f,p,k) \in \mathcal{I}^{(t)}} u_{p_i,p} \cdot k - \sum_{(f,s,p_i,k) \in \mathcal{I}^{(t)}} k. \quad (21)$$

Then, the firm adds a new order, $o(f, s, p, k_{f,p_i}^{(t)})$ to $\mathcal{I}^{(t)}$, where s is the firm’s default supplier for product p_i with probability p_{default} and, with probability $1 - p_{\text{default}}$, we select a supplier of p_i uniformly at random. We use $p_{\text{default}} = 0.8$, reflecting a strong level of “stickiness” in supplier-buyer relations, while allowing some randomness or one-off deals.

All completed orders at time t , $\mathcal{C}^{(t)}$, are reported as transactions for that timestep. The simulation also requires special logic, which we describe below, for products in Tier 0, which have no parts, and products in Tier $T + 1$ (the final tier), which are not used as parts for any other products and thus only bought by consumers.

Tier 0 products and exogenous supply. For each Tier 0 product p_0 , we define time-varying exogenous supply $supply(p_0, t)$, such that any firm f that supplies p_0 can only complete orders $o(b, f, p_0, k)$ where $k \leq supply(p_0, t)$. In the standard synthetic data (SS-std), exogenous supply is plentiful, so orders for Tier 0 products are completed almost immediately. However, we can also introduce supply shocks, which we model as follows: each Tier 0 product at each timestep t has an independent probability p_{shock} of experiencing a shock, at which point $supply(p_0, t) = supply_{\text{shock}}$. Then, we allow the supply to recover over the subsequent timesteps, by multiplying it in each timestep by some recovery rate $r > 1$, unless it experiences another shock.

In our synthetic data with shocks, SS-shocks, we use $p_{\text{shock}} = 0.01$, resulting in 10 shocks over 200 timesteps: shocks to product 0 at times 32 and 144, product 2 at times 42 and 155, product 3 at times 51, 90, and 144, and product 4 at times 16, 58, and 131. We allow a recovery rate of $r = 1.25$, resulting in a recovery time of approximately 30 timesteps from the initial shock to full recovery (since we set the stable supply to 1000x of $supply_{\text{shock}}$). In Figure 5, we visualize the number of transactions over time in each synthetic data (SS-std, SS-shocks, and SS-missing). While the missing firms reduce the number of transactions by a consistent fraction, the shocks dramatically disrupt the pattern of transactions, slowing them down whenever there is a shortage then trying to catch up whenever the Tier 0 products have recovered.

Final tier products and exogenous demand. For each product p in the final tier (i.e., Tier $T + 1$), we define time-varying exogenous demand $d(p, t)$, as well as firm-specific demand $d(f, p, t)$. To

simulate demand from consumers, with temporal patterns, we assign these products to one of three types: uniform, weekday, or weekend. We define demand as follows:

$$\nu \sim \mathcal{N}(0, 0.1) \quad (22)$$

$$\lambda = \begin{cases} 1 & \text{if type = uniform,} \\ 2 & \text{if type = weekday and } t \bmod 7 < 5, \\ 0.5 & \text{if type = weekday and } t \bmod 7 \geq 5, \\ 0.5 & \text{if type = weekend and } t \bmod 7 < 5, \\ 2 & \text{if type = weekend and } t \bmod 7 \geq 5. \end{cases} \quad (23)$$

$$d(p, t) = \lambda \cdot (d(p, t-1) + \nu) \quad (24)$$

$$d(f, p, t) = \text{Poisson}(d(p, t)) \quad (25)$$

In other words, ν captures random temporal drift and λ captures fixed weekly patterns, where uniform is the same over the week, weekday favors the first five days of the week, and weekend favors the last two days. Then, $d(f, p, t)$ is added as an order with buyer ‘‘consumer’’ to the incomplete orders $\mathcal{I}^{(t)}$ at the beginning of each timestep t . In our experiments, we allow demand to vary steadily like this, without any sharp changes, but it would be possible to simulate changes in consumer demand (e.g., due to new trends) by changing the demand schedule for final tier products.

C Details about experiments

Here we provide details about our experimental set-up, including our baselines and model training / testing procedures.

C.1 Production learning experiments

Temporal correlations. If product p_i is a part of product p_o , then we expect that some firms buy p_i and supply p_o , and it would be natural for those timeseries to be correlated, with buying slightly preceding supplying. So, for each product pair p_1 and p_2 , first we find all firms that buy p_1 and supply p_2 . If there is no such firm, then we give the pair a score of 0. If there are such firms, then for each firm f , we compute the buying timeseries of p_1 , i.e., the total amount bought by f of p_1 on $t = 1, 2, \dots$, along with the supply timeseries of p_2 , i.e., the total amount supplied by f of p_2 on $t = 1, 2, \dots$. Then, we compute the *maximum* correlation between the buying and supply timeseries, allowing the supplying timeseries to lag the buying timeseries by 0 to 7 timesteps. Finally, the score given to the pair is the average maximum correlation over firms that buy p_1 and supply p_2 .

Pointwise Mutual Information (PMI). If product p_i is a part of product p_o , then we would also expect that firms that supply p_o are unusually likely to buy p_i , compared to the base rate of firms buying p_i . This idea is naturally quantified by PMI, where we compare the joint probability to the product of the individual probabilities. Let $buy(p_1)$ represent whether a firm buys p_1 and $supply(p_2)$ represent whether a firm supplies p_2 . Then, we compute PMI as

$$PMI(p_1, p_2) = \log \left(\frac{\Pr(buy(p_1) \wedge supply(p_2))}{\Pr(buy(p_1)) \cdot \Pr(supply(p_2))} \right), \quad (26)$$

where the probabilities are computed as fractions of all firms.

node2vec. If product p_i is a part of product p_o , then we would also expect that the products are close to each other in embedding space. To test this, we train node2vec embeddings (Grover and Leskovec, 2016) on the firm-product graph, which is a static bipartite graph where an edge between a firm and a product indicates that the firm supplies or buys the product. We use embedding dimension 64 for the node2vec embeddings. Then, the score for product pair p_1, p_2 is the cosine similarity of their node2vec embeddings.

Inventory module. To learn production functions, we train our inventory module on the transactions data (only the train set, for consistency with the edge prediction experiments) and update it according to the inventory loss (6). In practice, we find it effective to choose a debt penalty λ_{debt} that is 25% larger than the consumption reward λ_{cons} , as reported in Table 4. We experiment with learning

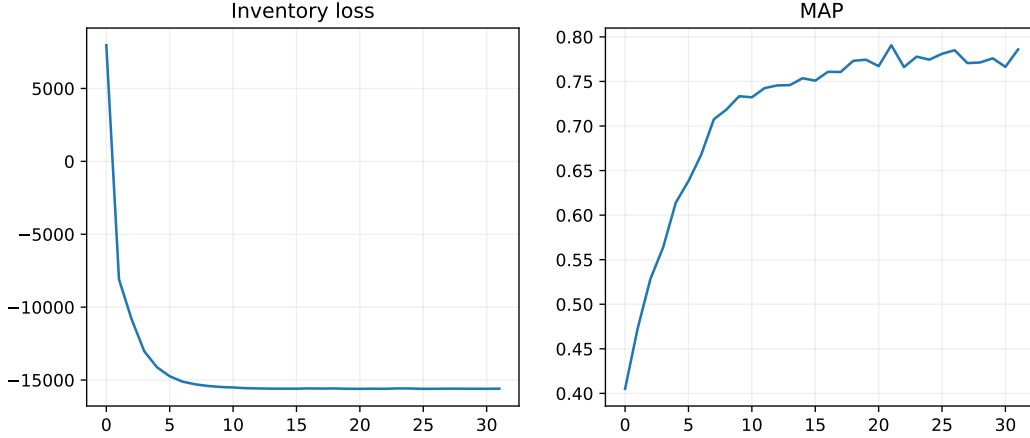


Figure 6: Comparing inventory module’s loss (6) vs. MAP on ground-truth production functions, trained on SS-std.

| | Synthetic data | Tesla | IED |
|--|----------------|-------|----------------------------------|
| SC-TGN | | | |
| Memory dimension | 500 | 1000 | 1000 |
| Embedding dimension | 500 | 1000 | 1000 |
| Time dimension | 100 | 100 | 100 |
| # neighbors for node embedding | 20 | 20 | 100 |
| Update penalty λ_{update} | 1 | 1 | 1 |
| SC-GraphMixer | | | |
| # MLP Mixer layers | 2 | 2 | 2 |
| Node encoding dimension | 500 | 50 | 300 |
| Link encoding dimension | 100 | 10 | 10 |
| # neighbors for node encoding | 20 | 100 | 10 |
| # neighbors for link encoding | 20 | 10 | 2 |
| Inventory module | | | |
| Debt penalty λ_{debt} | 5 | 5 | 5 |
| Consumption reward λ_{cons} | 4 | 4 | 4 |
| Adjustment penalty λ_{adjust} | 4 | 4 | 4 |
| Training parameters | | | |
| Batch size | 30 | 30 | 100 (SC-TGN), 30 (SC-GraphMixer) |
| Learning rate | 0.001 | 0.001 | 0.001 |
| Max # epochs | 100 | 100 | 100 |
| Patience | 10 | 10 | 10 |

Table 4: Hyperparameters that we used in our experiments.

the inventory module’s attention weights directly and with product embeddings, following (4). We experiment with product embeddings from node2vec, from a simple GNN trained on link prediction over the collapsed product-product graph (collapsed from the firm-product graph, so an edge from product p_1 to p_2 indicates how often a firm buys p_1 and supplies p_2), and from SC-TGN. We find that product embeddings from node2vec help the inventory module the most on synthetic data and embeddings from the simple GNN help it the most on the microscope dataset. In Figure 6, we also show that our inventory loss (6) is well-correlated with MAP, despite the inventory loss not having access to any ground-truth parts.

C.2 Edge prediction experiments

Model training. As discussed in the main text, for all datasets, we order transactions chronologically and split them into train (70%), validation (15%), and test (15%). In these experiments, we train the models on the train set, choose hyperparameters based on the validation set, and report final results on

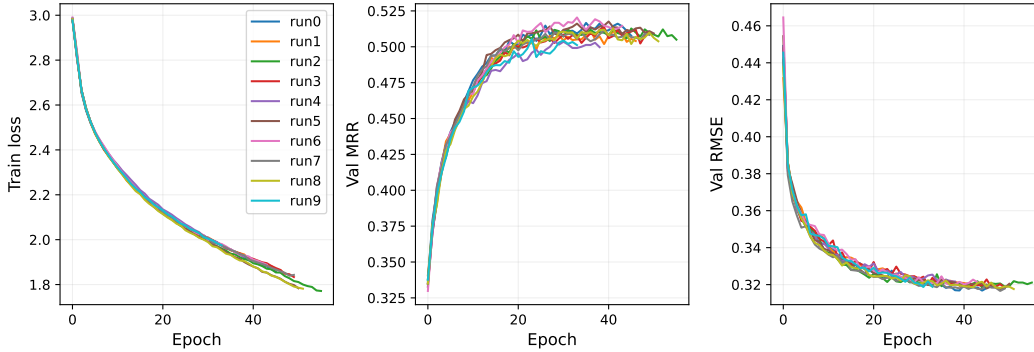


Figure 7: Performance over 10 random seeds of SC-TGN on SS-std.

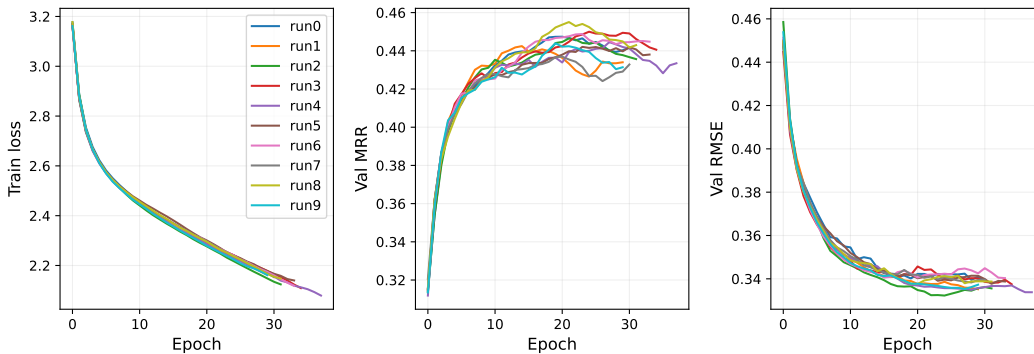


Figure 8: Performance over 10 random seeds of SC-GraphMixer on SS-std.

the test set. When training the models, we train for a maximum of 100 epochs, but we allow for early stopping, if the validation MRR does not improve for over 10 epochs. In our main experiments (Table 2), we tested the following models: Edgebank, Static, Graph Transformer, SC-TGN, SC-TGN+inv, SC-GraphMixer, and SC-Graphmixer+inv. In Table 4, we report the hyperparameters we used for SC-TGN and SC-GraphMixer, which we found by sweeping over the hyperparameters. For all experiments, we ran 10 trials, each with a different random seed, and reported the mean and standard deviation in test MRR and test RMSE. As shown by the small standard deviations, performance is quite stable over random seeds, which we also show in Figures 7-8. These figures also show that SC-TGN and SC-Graphmixer both make steady progress in train and validation metrics over epochs: train loss decreases, validation MRR increases, and validation RMSE decreases. It is reassuring to see that the improvements in train loss correspond well to improvements in validation MRR and RMSE, since the train loss (16) combines multiple objectives, and, furthermore, we cannot directly train on MRR, which is non-differentiable, so instead we use softmax cross-entropy as a proxy loss.

Ablations. We can view the Static and Graph Transformer baselines as ablations of our models, so we used the SC-TGN hyperparameters wherever applicable for fair comparison (e.g., embedding dimension, batch size). Since SC-TGN learns the initial memory, the Static baseline is equivalent to SC-TGN if no memory updates are applied and the embedding module is ID. The Static baseline is also a nested version of SC-GraphMixer, when we allow SC-GraphMixer to learn its initial node features. The Graph Transformer baseline is equivalent to SC-TGN if no memory updates are applied and the embedding module is UniMP (Shi et al., 2021). Since SC-TGN was our best-performing model, we also ran further ablations of SC-TGN to test the value of our extensions. We compared it to the original TGN, where we stripped away most of the extensions discussed in Appendix A.1: it no longer predicted edge weight, we removed the update penalty and learnable initial memory, and we trained it only on perturbation negatives. We also compared it to a version of SC-TGN that applied memory updates, but used ID for the embedding module, i.e., uses the node memory directly instead of applying a GNN to the memories. As shown in Table 5, we found that SC-TGN greatly outperformed both of these ablations as well.

| | Tesla | IED |
|-------------|----------------------|----------------------|
| TGN | 0.612 (0.009) | 0.582 (0.016) |
| SC-TGN (id) | 0.537 (0.021) | 0.422 (0.015) |
| SC-TGN | 0.820 (0.007) | 0.842 (0.004) |

Table 5: Ablations of SC-TGN: comparing to original TGN (Rossi et al., 2020) and SC-TGN with ID embeddings, i.e., use memory directly as embedding, instead of applying GNN to memories. We only evaluate edge existence here, with mean reciprocal rank (MRR \uparrow), and leave out edge weight, since the original TGN did not predict edge weight. We report mean and standard deviation (in parentheses) over 10 seeds.

| | SS-std | SS-shocks | SS-missing |
|--------------------|----------------------|----------------------|----------------------|
| SC-TGN | 0.522 (0.003) | 0.449 (0.004) | 0.494 (0.004) |
| SC-TGN+inv* | 0.548 (0.003) | 0.474 (0.003) | 0.476 (0.003) |
| SC-GraphMixer | 0.453 (0.005) | 0.426 (0.004) | 0.446 (0.003) |
| SC-GraphMixer+inv* | 0.477 (0.005) | 0.450 (0.005) | 0.430 (0.003) |

Table 6: Testing the impact of inventory module on edge existence prediction, when the inventory module is provided the ground-truth production functions. We report mean and standard deviation (in parentheses) over 10 seeds.

Analysis of +inv experiments. For the +inv experiments, we found that validation performance was best if we first pretrained the inventory module on only inventory loss (6), then co-trained the inventory module and SC-TGN / SC-GraphMixer, following the joint loss (16). Furthermore, in the +inv experiments, we experimented with whether to include the inventory module’s edge prediction penalties or not (8)-(9). Based on validation performance, we found that the penalties were useful on synthetic data, in the standard setting and under supply shocks, but not when there were missing transactions, or for the real-world datasets, so for those, we turned off the penalties. We believe this is because, while the inventory module is robust to missing transactions when learning production functions (as shown by our production learning results in Table 1), the penalties are not robust to missing transactions, since they rely on having an approximately correct and complete inventory. For example, if product p_i is an input part to product p_o , and we are missing transactions where firm f receives p_i , then the inventory module will incorrectly believe that f has zero inventory of p_i and penalize transactions where f is supposed to supply p_o .

To test this theory, we experimented with providing the inventory module with the *ground-truth* production functions, and tested the usefulness of the edge prediction penalties on the three synthetic datasets. We found that, on SS-std and SS-shocks, the penalties help SC-TGN and SC-GraphMixer achieve stronger performance on both edge existence and edge weight prediction, but for SS-missing, performance worsens (Table 6). These results show that the penalties hurting edge prediction performance are *not* indicative of how well the inventory module has learned the production functions, since here we provided the ground-truth production functions. Rather, missingness in the synthetic data causes the penalties to hurt, not help, performance. This analysis motivates the need to explore penalties in the future that are more robust to missingness, as discussed in Appendix A.3, so that even with missing data, the inventory module can not only learn production functions, but also aid edge prediction so that the two objectives become more synergistic.